Eur. Phys. J. C (2025) 85:248
https://doi.org/10.1140/epjc/s10052-025-14001-7

THE EUROPEAN PHYSICAL JOURNAL C

Regular Article - Theoretical Physics

Anisotropic dark matter stars in gravity's rainbow

Takol Tangphati[1,2,a], **İzzet Sakallı**[3,b], **Ayan Banerjee**[4,c], **Javlon Rayimbaev**[5,6,d]

[1] School of Science, Walailak University, Thasala, Nakhon Si Thammarat 80160, Thailand
[2] Research Center for Theoretical Simulation and Applied Research in Bioscience and Sensing, Walailak University, Thasala 80160, Thailand
[3] Physics Department, Eastern Mediterranean University, via Mersin 10, 99628 Famagusta, North Cyprus, Turkey
[4] Atrophysics Research Centre, School of Mathematics, Statistics and Computer Science, University of KwaZulu-Natal, Private Bag X54001, Durban 4000, South Africa
[5] New Uzbekistan University, Movarounnahr Street 1, 100000 Tashkent, Uzbekistan
[6] Urgench State University, Kh. Alimjan Str. 14, 221100 Urgench, Uzbekistan

Received: 17 January 2025 / Accepted: 22 February 2025

Abstract In this study, we explore the structural and stability properties of anisotropic dark matter stars within the framework of gravity's rainbow. By incorporating energy-dependent rainbow functions into the spacetime metric, we examine quantum gravitational effects on compact stars under extreme conditions. Utilizing a modified Tolman–Oppenheimeer–Volkoff (TOV) formalism, we derive exact analytical solutions and perform numerical simulations to investigate the impact of anisotropy and rainbow parameters on stellar mass, radius, and compactness. Our analysis includes stability criteria such as the static stability condition, adiabatic indices, and sound speed causality, highlighting the dynamic behavior of these stars. The findings reveal that gravity's rainbow allows for more massive and stable compact stars compared to General Relativity, offering insights into quantum gravitational corrections and their astrophysical implications.

1 Introduction

The exploration of anisotropic compact stars [1–5] has become a focal point of contemporary astrophysical research, largely due to their potential to unravel the mysteries of extreme gravitational environments and the fundamental interactions shaping them. Within the framework of modified theories of gravity [6–9], the study of compact objects gains additional significance as a testing ground for deviations from General Relativity (GR). In this context, the concept of gravity's rainbow, originally proposed to incorporate quantum gravitational effects at the Planck scale, offers a compelling avenue for understanding the intricate behavior of stellar structures under extreme conditions [10–12].

Gravity's rainbow modifies the spacetime metric by introducing energy-dependent rainbow functions, $\Xi(x)$ and $\Sigma(x)$, where $x = E/E_p$ represents the ratio of particle energy E to the Planck energy E_p. These functions alter the relativistic dispersion relations, enabling the study of quantum gravitational effects in high-energy regimes [13,14]. Compact stars, especially those composed of dark matter, are ideal candidates for investigating such effects, as they represent environments where gravitational and quantum effects interplay significantly [15–20].

Anisotropy, characterized by unequal radial (P_r) and tangential ($P_\perp$) pressures, naturally arises in compact stars due to factors such as phase transitions, electromagnetic fields, and density gradients [21,22]. In the context of gravity's rainbow, anisotropic stars provide a unique platform for analyzing how modified spacetime geometries influence stellar equilibrium, stability, and observable properties. Recent studies have demonstrated that anisotropic models can better accommodate astrophysical observations, such as the mass-radius relationship of neutron stars, compared to isotropic models [23–27].

Our motivation stems from the need to explore the interplay between anisotropy and quantum gravitational corrections in compact stars. Dark matter stars, hypothesized to be composed of exotic matter, serve as ideal systems for such an investigation. By incorporating a polytropic equation of state that accounts for anisotropy, we aim to elucidate the impact of gravity's rainbow on the structural and stability charac-

[a] e-mail: takoltang@gmail.com
[b] e-mail: izzet.sakalli@emu.edu.tr
[c] e-mail: ayanbanerjeemath@gmail.com (corresponding author)
[d] e-mail: javlon@astrin.uz

Published online: 09 March 2025

teristics of these stars [28–30]. Additionally, the inclusion of anisotropy as an extra matter component offers a versatile framework for analyzing the deviations introduced by rainbow gravity [31,32].

This paper is organized as follows: in Sect. 2, we present the field equations governing the structure of anisotropic stars in the context of gravity's rainbow. Section 3 provides a detailed review of gravity's rainbow and the modified TOV equations. Section 4 is dedicated to numerical results and discussions, where we analyze the dependence of stellar properties on the rainbow parameters Σ and the anisotropy parameter β. The stability analysis, including the static stability criterion, adiabatic indices, and sound speed causality, is presented in Sect. 5. Finally, we summarize our findings and propose future research directions in Sect. 6.

2 Equation of state and setup

In this section, we establish the equation of state (EoS) and the anisotropic profile used in the analysis, inspired by the theoretical framework discussed in [33]. Boson stars are intriguing self-gravitating configurations, which can be composed of either spin-zero fields (scalar boson stars) [34] or spin-one fields (Proca stars) [17,35,36]. Earlier works [37,38] demonstrated the maximum mass attainable by scalar boson stars without self-interactions, while later studies [29,39] revealed that self-interactions significantly influence the maximum mass. According to [40], scalar boson stars reach their maximum mass in systems without interactions. However, as noted in [29,41–44], self-interactions can notably alter these stars' mass.

A canonical complex scalar field, φ, is governed by the Einstein-Klein-Gordon action:

$$S = \int d^4x\sqrt{-g}\left(\frac{R}{16\pi} + \mathcal{L}_M\right), \tag{1}$$

$$\mathcal{L}_M = -g^{\mu\nu}\partial_\mu\varphi\partial_\nu\varphi^* - V(|\varphi|), \tag{2}$$

where g is the determinant of the metric tensor $g_{\mu\nu}$, R is the Ricci scalar, $\mathcal{L}_M$ is the Lagrangian density of the matter content, and $V(|\varphi|)$ denotes the scalar potential [42].

For static, spherically symmetric configurations, the scalar field is parametrized as follows:

$$\varphi(r,t) = \psi(r)\exp(-i\varpi t), \tag{3}$$

where ϖ is a real parameter corresponding to the oscillation frequency [42].

Although the scalar field depends on time, the resulting stress-energy tensor remains time-independent. Consequently, Einstein's field equations for an anisotropic fluid take the standard form, where the energy density is given by [2,44]:

$$\rho = \varpi^2 e^{-2\nu}\psi^2 + e^{-2\lambda}\psi'^2 + V(\psi), \tag{4}$$

and the radial and tangential pressures are expressed as:

$$P_r = \varpi^2 e^{-2\nu}\psi^2 + e^{-2\lambda}\psi'^2 - V(\psi), \tag{5}$$

$$P_\perp = \varpi^2 e^{-2\nu}\psi^2 - e^{-2\lambda}\psi'^2 - V(\psi). \tag{6}$$

The anisotropy factor, defined as the difference between tangential and radial pressures, is given by:

$$\sigma \equiv P_\perp - P_r = -2e^{-2\lambda}\psi'^2 < 0. \tag{7}$$

This negative anisotropy is characteristic of boson stars [30].

Under specific conditions, the anisotropy can be negligible, allowing the system to be approximated as isotropic. A particular model assumes the scalar potential:

$$V(|\varphi|) = m_x^2|\varphi|^2 + \frac{\varkappa}{2}|\varphi|^4, \tag{8}$$

where m_x is the scalar field mass, and $\varkappa$ is the self-interaction coupling constant. The corresponding EoS is described by [29]:

$$P_r = \frac{\rho_0}{3}\left(\sqrt{1+\frac{\rho}{\rho_0}} - 1\right)^2, \tag{9}$$

with ρ_0 defined as:

$$\rho_0 = \frac{m_x^4}{3\varkappa}. \tag{10}$$

This EoS is valid for approximately isotropic boson stars, provided the condition:

$$\frac{\varkappa}{4\pi} \gg m_x^2, \tag{11}$$

is satisfied [28].

The EoS recovers well-known limits in specific regimes. For dilute stars [30]:

$$P_r \approx \frac{\rho^2}{12\rho_0}, \quad \rho \ll \rho_0, \tag{12}$$

and in the ultra-relativistic limit:

$$P_r \approx \frac{\rho}{3}, \quad \rho \gg \rho_0. \tag{13}$$

The equation of state of a Bose–Einstein condensate is expressed in polytropic form:

$$P_r = K\rho^2, \tag{14}$$

where K is the proportionality constant related to the mass m and the scattering length a as:

$$K = \frac{2\pi a}{m_x^3}. \tag{15}$$

Let us define $K = \frac{z}{B}$, where z is dimensionless and B is a pressure-related dimension. For convenience, one can set $z = 0.05$ and $B = 66\,[\mathrm{MeV/fm^3}]$ [45,46]. However, it is also worth noting that there are other studies that suggest this aligns with neutron and quark star energy densities, with $B \approx (150\ \mathrm{MeV})^4$ [47,48].

Finally, we consider an anisotropy factor [22,23,49–51]:

$$\sigma = \beta P_r \left(1 - e^{-2\lambda}\right). \tag{16}$$

where β is a dimensionless prefactor ensuring dimensional consistency and vanishing anisotropy at the center and surface of the star. In non-relativistic regimes, $1 - e^{-\lambda} \ll 1$ implies $\sigma \sim 0$. Since $P_r > P_\perp$ (Eqs. 5 and 6), $\beta < 0$ is required to maintain $\sigma < 0$. Thus, in our numerical analysis, we consider β within the range $[-2, 0]$.

In summary, this section presents the foundation for studying boson stars with anisotropic matter and explores the influence of the EoS and anisotropy on stellar properties.

3 Review of gravity's rainbow and stellar structure equations

3.1 Rainbow theory

Since the concept of doubly special relativity (DSR) was introduced by Amelino-Camelia [10] as a generalization of special relativity, further details can be found in Ref. [13]. In this theory, two fundamental constants, the speed of light c and the Planck energy E_p, are referred to as "doubly special." Although DSR has achieved significant milestones, it faces unresolved challenges, such as the so-called "soccer ball" problem. To address this issue, Magueijo and Smolin [11] extended DSR to curved spacetimes, proposing a framework called rainbow gravity (or gravity's rainbow). This framework is based on the assumption that the background spacetime depends on the energy of a test particle.

In this context, particles with different energies perceive unique distortions of spacetime, modifying the conventional relativistic dispersion relation at high-energy scales, specifically near the Planck scale. The modified dispersion relation is given by

$$E^2 \Xi(x)^2 - p^2 \Sigma(x)^2 = m^2, \tag{17}$$

where $\Xi(x)$ and $\Sigma(x)$ are the so-called rainbow functions, defined in terms of the dimensionless ratio $x = E/E_p$. Here, E and E_p represent the relativistic total energy of the probe particle and the Planck energy, respectively. The rainbow functions have distinct forms and are responsible for altering the ultraviolet regime of spacetime, contributing significantly to the structure of rainbow gravity. At low-energy scales, characterized by $x = E/E_p \to 0$, the rainbow functions satisfy

$$\lim_{x\to 0} \Xi(x) = 1, \quad \lim_{x\to 0} \Sigma(x) = 1, \tag{18}$$

and the standard energy dispersion relation is recovered. The selection of rainbow functions is crucial as it determines the quantum gravitational modifications to spacetime. A widely used choice is given by $\Xi(x) = 1$ and $\Sigma(x) = \sqrt{1 - \eta x^n}$, where η and n are dimensionless parameters that introduce deviations from General Relativity while preserving consistency in the low-energy regime. Another common alternative, derived from deformed Lorentz transformations in DSR, takes the form $\Xi(x) = \Sigma(x) = \frac{1}{1+\lambda x}$. Both choices have been extensively explored in astrophysical scenarios [12,20]. In this study, we adopt the former form due to its analytical tractability and its capability to capture essential quantum gravity effects in stellar structure equations.

The metric in rainbow gravity, $g^{\mu\nu}(x)$, is written as [11]

$$g^{\mu\nu}(x) = \eta^{ab} e_a^\mu(x) \otimes e_b^\nu(x), \tag{19}$$

where $e_a^\mu(x)$ represents the energy-dependent vierbein fields, related to the energy-independent tetrads $\tilde{e}_a^\mu$ by the relations

$$e_0^\mu(x) = \frac{1}{\Xi(x)} \tilde{e}_0^\mu, \quad e_k^\mu(x) = \frac{1}{\Sigma(x)} \tilde{e}_k^\mu, \tag{20}$$

where the spatial indices k take values $(1, 2, 3)$. The tilde denotes the energy-independent tetrads. Note that the rainbow functions, which are implicitly dynamical functions of the coordinates, modify not only the relativistic dispersion relation but also the metric structure of spacetime.

Rainbow gravity has emerged as a plausible framework for investigating quantum gravitational effects in highly dense and compact stellar objects. Within this framework, the equation of motion takes the form [11]

$$G_{\mu\nu}(x) \equiv R_{\mu\nu}(x) - \frac{1}{2} g_{\mu\nu}(x) R(x) = k(x) T_{\mu\nu}(x), \tag{21}$$

where $T_{\mu\nu}(x)$ represents the stress-energy tensor, which acts as the source of spacetime curvature, and $G_{\mu\nu}(x)$ is the Einstein tensor. The term $k(x) = 8\pi G(x)$ introduces an energy-dependent gravitational coupling constant. For simplicity, we work in units where $G(x) = 1$.

3.2 Modified TOV equations of gravity's rainbow

Here, we derive the equations of hydrostatic equilibrium in the framework of rainbow gravity, under the assumption of a static, four-dimensional spherically symmetric metric, which is modified as a rainbow metric in the following form [11]:

$$ds^2 = -\frac{e^{2\nu(r)}}{\Xi^2(x)} dt^2 + \frac{e^{2\lambda(r)}}{\Sigma^2(x)} dr^2 + \frac{r^2}{\Sigma^2(x)} d\Omega^2, \tag{22}$$

where the functions $\nu(r)$ and $\lambda(r)$ depend on the radial coordinate r, and $d\Omega^2$ is defined as $d\Omega^2 = d\theta^2 + \sin^2\theta\, d\phi^2$. The rainbow functions $\Xi(x)$ and $\Sigma(x)$ depend on the dimensionless energy ratio $x = E/E_p$ and are independent of the spacetime coordinates (r, t, θ, ϕ).

Inspired by [14], we investigate the possible existence of exotic stars composed of anisotropic matter in the context of rainbow gravity. To describe the matter distribution, we use

the following energy-momentum tensor [15]:

$$T_{\mu\nu} = (\rho + P_\perp)u_\mu u_\nu + P_\perp g_{\mu\nu} - (P_\perp - P_r)\chi_\mu \chi_\nu, \quad (23)$$

where $\rho(r)$ is the energy density, $P_r(r)$ is the radial pressure, and $P_\perp(r)$ is the tangential pressure. The fluid is assumed to be at rest, so the four-velocity of the fluid is given by

$$u^\mu = \left(\frac{\Xi(x)}{e^{\nu(r)}}, 0, 0, 0\right), \quad (24)$$

with the condition $u_\mu u^\mu = -1$. The unit normal vector in the radial direction is represented as χ_μ, satisfying $\chi_\mu \chi^\mu = 1$.

By introducing a new variable, $e^{-2\lambda(r)} = 1 - \frac{2M_{\rm eff}(r,x)}{r}$, the modified TOV equations for a static, spherically symmetric spacetime can be written using the metric (22) and the stress-energy tensor (23) in the following form [12]:

$$M_{\rm eff}(r,x) = \int_0^r \frac{4\pi r^2 \rho(r)}{\Sigma^2(x)} dr \equiv \frac{m(r)}{\Sigma^2(x)}, \quad (25)$$

$$P_r' = -(\rho + P_r)\nu' + \frac{2}{r}(P_\perp - P_r), \quad (26)$$

$$\nu'(r) = \frac{M_{\rm eff}(r,x)\Sigma^2(x) + 4\pi r^3 P_r(r)}{r\,(r - 2M_{\rm eff}(r,x))\,\Sigma^2(x)}, \quad (27)$$

where the prime denotes differentiation with respect to the radial coordinate r. Now we are in a position to solve the differential equations (25)–(27) for the specified EoSs under appropriate boundary conditions.

4 Numerical results and discussions

In this section, we examine the physical characteristics of anisotropic dark matter stars within the framework of rainbow gravity. Using the given equations of state (EoS) in Eqs. (14) and (16), we explore the interior solutions by numerically solving the modified TOV equations, Eqs. (25)–(27). The numerical approach relies on initial conditions specified at the star's center ($r = 0$), such that $m(0) = 0$ and $\rho(0) = \rho_c$, where ρ_c represents the central energy density. Additionally, at the surface of the star ($r = R$), the boundary conditions $P_r(R) = P_\perp(R) = 0$ are satisfied, and the total mass of the star is given by $M = m(r = R)$. We present our findings by analyzing the impact of the rainbow parameter Σ and the anisotropy parameter β. Furthermore, we assess the stability of the star's configuration using the static stability criterion, the adiabatic index, and the speed of sound. In the following discussion, the radius of the star is expressed in kilometers (km), the bag constant is measured in MeV/fm^3, and the stellar mass is given in solar masses ($M_\odot$).

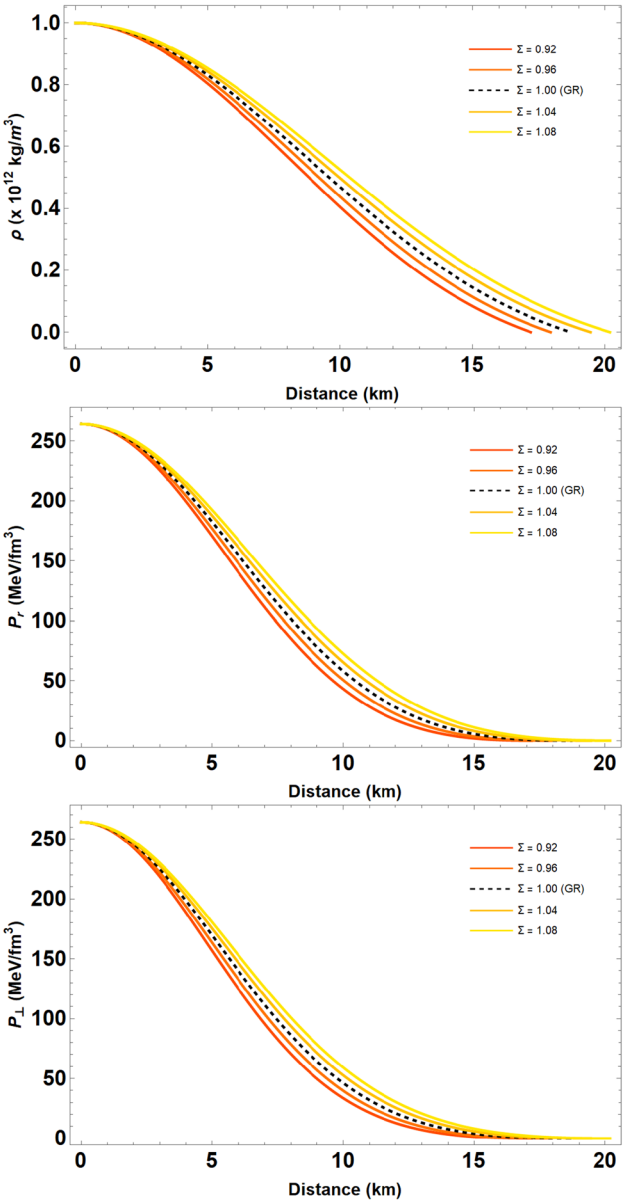

Fig. 1 From top to bottom, we present the energy density ρ, radial pressure P_r, and transverse pressure $P_\perp$ as functions of the radial coordinate r. The range of values for Σ is $\Sigma \in [0.9, 1.1]$, while the other parameters are fixed as $B = 70$ MeV/fm^3, $\beta = -0.5$, and $z = 0.05$. The GR result is shown by a black dashed line

4.1 Profiles for variation of Σ

To analyze the effects of the rainbow parameter Σ on the stellar structure, we compute the stellar properties for $\Sigma \in [0.9, 1.1]$, while keeping the other parameters fixed as $B = 70$ MeV/fm^3, $\beta = -0.5$, and $z = 0.05$. Figure 1 depicts the variation of energy density ρ, radial pressure P_r, and transverse pressure $P_\perp$ with respect to the radial coordinate r. For comparison, we include the case of pure GR, corresponding to $\Sigma = 1.0$ (Fig. 2).

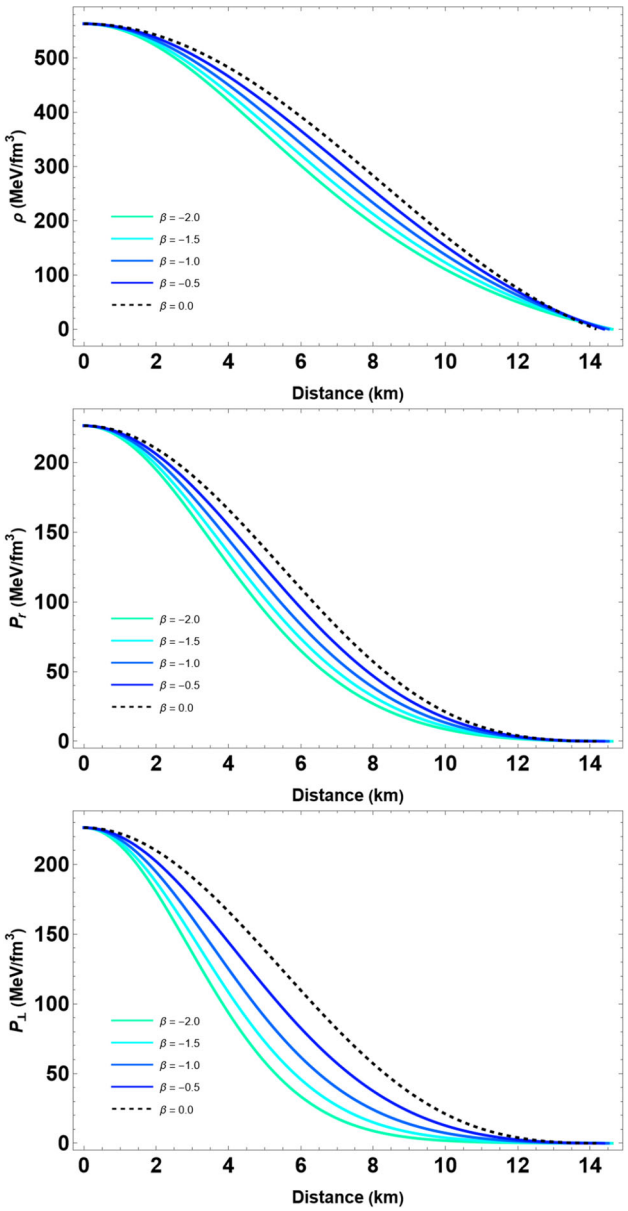

Fig. 2 From top to bottom, we present the energy density ρ, radial pressure P_r, and transverse pressure $P_\perp$ as functions of the radial coordinate r. The range of values for β is $\beta \in [-2.0, 0.0]$, while the other parameters are fixed as $B = 70$ MeV/fm^3, $\Sigma = 0.8$, and $z = 0.05$. A black dashed line represents the isotropic solution

We further examine the mass-radius ($M - R$) and mass-compactness ($M - M/R$) relations in Fig. 3. The numerical results, summarized in Table 1, show that the maximum mass and the corresponding radius increase with larger values of Σ. For instance, the maximum mass reaches $M_{\max} = 3.38 M_\odot$ with a radius of $R = 20.19$ km at $\Sigma = 1.08$. This indicates that rainbow gravity predicts more massive compact stars compared to GR when $\Sigma > 1$.

Additionally, the variation of the maximum compactness for different Σ values is illustrated in the lower panel of Fig. 3.

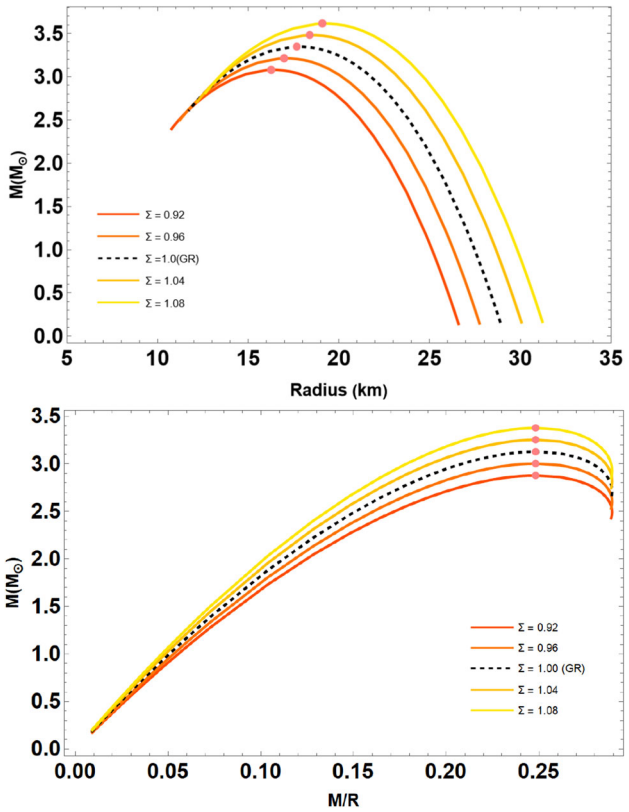

Fig. 3 The effects of the rainbow function on the mass-radius and maximum compactness relations for dark matter compact stars. The results are derived using the parameter values from Fig. 1. The GR result is shown by a black dashed line

As observed in Table 1, the maximum compactness M/R remains constant at $M/R = 0.248$, satisfying the Buchdahl limit $M/R < 4/9$. This ensures that the considered configurations do not form apparent horizons, thereby classifying them as stable compact objects rather than black holes. However, highly compact configurations such as ultracompact stars or gravastars remain interesting possibilities for further study [49,52]. Additionally, compactness plays a crucial role in gravitational wave emission, as more compact objects may exhibit modified quasi-normal mode frequencies, providing observational tests for quantum gravity-inspired deviations [53]. These results suggest that Σ significantly influences the overall mass and size of the star while maintaining the stability criterion.

4.2 Profiles for variation of β

Figure 2 demonstrates the effect of the anisotropy parameter β on ρ, P_r, and $P_\perp$ for the structure of the stars, with the isotropic case shown for comparison. Parameter sets represent varying values for $\beta \in [-2.0, 0.0]$ with the corresponding values being $B = 70$ MeV/fm^3, $z = 0.05$, and $\Sigma = 0.8$. Further, we show the ($M - R$) and ($M - M/R$) relations in

Table 1 Structural properties of dark matter stars for $B = 70$ MeV/fm^3, $z = 0.05$, $\beta = -0.5$, and varying $\Sigma \in [0.9, 1.1]$

Σ	M [$M_\odot$]	R_M [km]	ρ_c [MeV/fm^3]	M/R
0.92	2.88	17.20	563	0.248
0.96	3.00	17.95	563	0.248
1.0 (GR)	3.13	18.69	563	0.248
1.04	3.25	19.44	563	0.248
1.08	3.38	20.19	563	0.248

Table 2 A summary of the structural properties of dark matter stars for $B = 70$ MeV/fm^3, $z = 0.05$, $\Sigma = 0.8$, and different values of $\beta \in [-2.0, 0.0]$

β	M [$M_\odot$]	R_M [km]	ρ_c [MeV/fm^3]	M/R
-2.0	1.83	13.43	863	0.202
-1.5	1.98	13.88	713	0.212
-1.0	2.14	13.76	713	0.231
-0.5	2.31	13.56	713	0.253
0.0	2.50	14.17	562	0.260

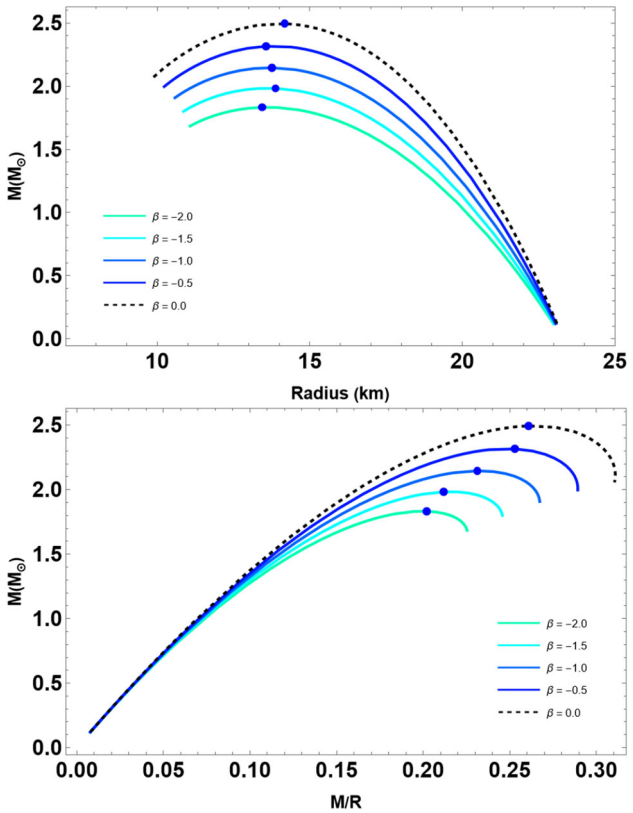

Fig. 4 The effects of the anisotropy parameter β on the mass-radius and maximum compactness relations for dark matter compact stars. The results are derived using the parameter values from Table 2. A black dashed line represents the isotropic solution

Fig. 4. As we are dealing with dark matter stars, we consider a set of negative values of β; see Sect. 2 for further details. The influence of β on the $(M - R)$ relations is substantial, with higher values of β correlating with increased maximum masses. It can be observed from Table 2 that the maximum mass goes up to $M_{\max} = 2.31 M_\odot$ for $\beta = -0.5$ with a maximum radius of $R_{\max} = 14.17$ km. In addition, the highest mass of dark matter stars at $\beta = 0$ (isotropic solution for rainbow gravity) is noted to be $2.50 M_\odot$. The intriguing feature of the dark matter model is that isotropic solutions possess a greater mass than their anisotropic counterparts when $\beta < 0$ is considered (see Fig. 4). Subsequently, we illustrate the influence of β on the characteristics of the $(M - M/R)$ relations in the lower panel of Fig. 4. According to Table 2, the maximum compactness of the star increases with β, and at $\beta = -0.5$, this value could be $M/R = 0.260$.

5 Stability analysis of anisotropic quark stars

In this section, we aim to evaluate the stability of our proposed model. To achieve this, we employ the static stability criterion, the adiabatic index, and the speed of sound. Each of these stability conditions is systematically examined and graphically illustrated.

5.1 Static stability criterion

Here, we analyze the stability of equilibrium configurations within the framework of rainbow gravity, focusing on the *static stability criterion* discussed in [54,55]. The results are presented in the $M - \rho_c$ plane, where M is the gravitational mass and ρ_c is the central energy density. While this criterion has been extensively studied in the context of GR, it also finds relevance in modified gravity theories, as discussed in [56–59]. The criterion is expressed as:

$$\frac{dM}{d\rho_c} < 0 \rightarrow \text{unstable configuration}, \tag{28}$$

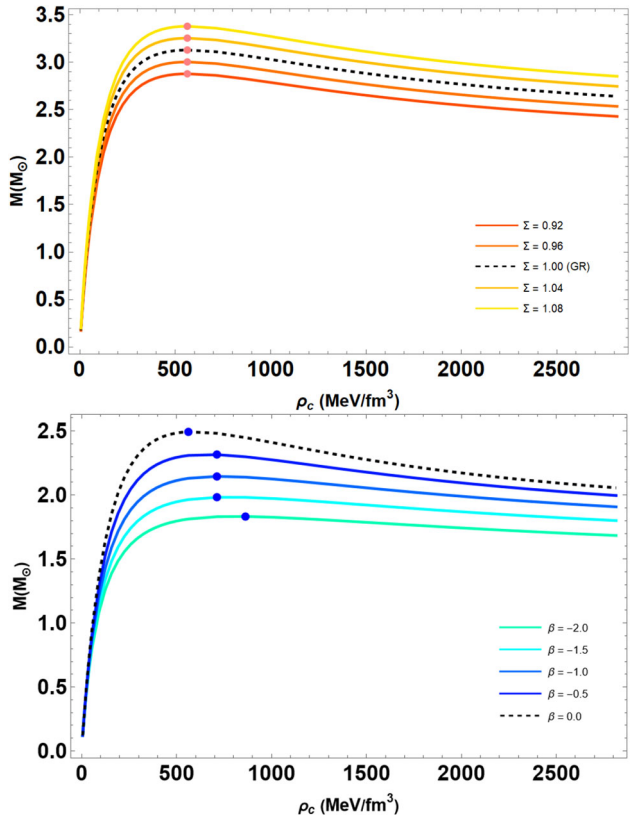

Fig. 5 The $M - \rho_c$ curves for a family of anisotropic dark matter stars with variations in Σ and β

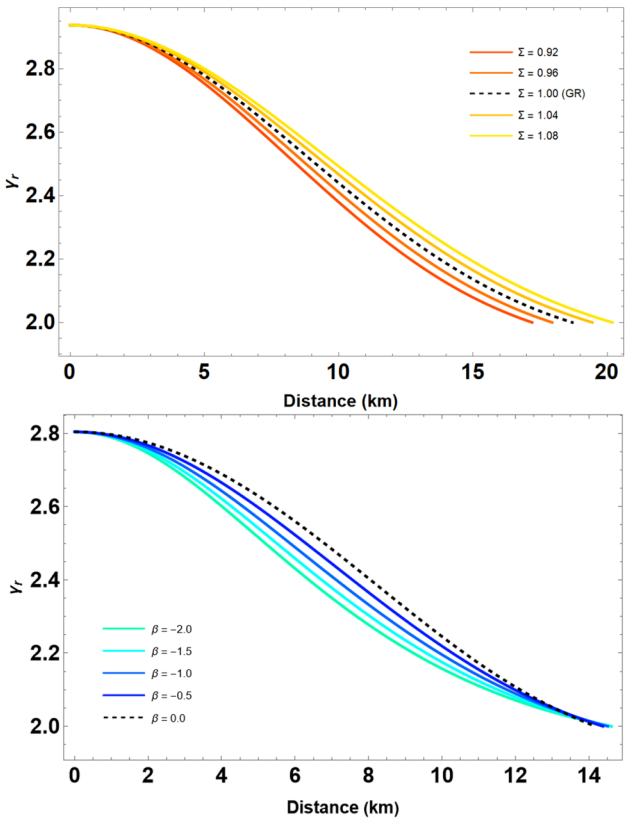

Fig. 6 The adiabatic index γ as a function of radius for anisotropic dark matter stars with variations in Σ and β

$$\frac{dM}{d\rho_c} > 0 \rightarrow \text{stable configuration.} \tag{29}$$

It should be noted that this is a necessary but not sufficient condition for stability. The mass-central density relations are illustrated in Fig. 5 for each case considered. The pink and blue points in Fig. 5 denote the transition from stable to unstable configurations, where $dM/d\rho_c = 0$, with $dM/d\rho_c > 0$ indicating stability.

5.2 Adiabatic indices

We now examine the dynamical stability of the astrophysical models by analyzing the behavior of the adiabatic index, γ. This concept, first introduced by Chandrasekhar [60], evaluates the stability of equilibrium configurations. Recent studies, such as [61], have extended this analysis to the framework of rainbow gravity. The radial adiabatic index γ is defined as:

$$\gamma \equiv \left(1 + \frac{\rho}{P_r}\right)\left(\frac{dP_r}{d\rho}\right)_S, \tag{30}$$

where $dP_r/d\rho$ represents the derivative of the radial pressure with respect to energy density, and the subscript S denotes constant entropy. The critical adiabatic index for stability is $\gamma_{cr} = 4/3$, as derived for isotropic fluid spheres [62]. For stability, the condition $\gamma > \gamma_{cr}$ must hold. Using Eq. (30), Fig. 6 depicts how γ varies with radius for several representative values of Σ and β. The results indicate that γ decreases monotonically with r but remains above γ_{cr}, suggesting a dynamically stable configuration.

5.3 Sound speed and causality

Finally, we evaluate the stability of exotic stars by analyzing the speed of sound, which satisfies the following equation:

$$v^2_{r,\perp} = \frac{dP_{\{r,\perp\}}}{d\rho}. \tag{31}$$

It is crucial to ensure that the sound speed remains below the speed of light, as expressed by the condition:

$$v^2_{r,\perp} < 1. \tag{32}$$

To verify this, we examine the speed of sound in dark matter stars and present the results in Figs. 7 and 8, which illustrate the radial and transverse sound speeds for several representative values of Σ and β, as provided in Tables 1 and 2, respectively.

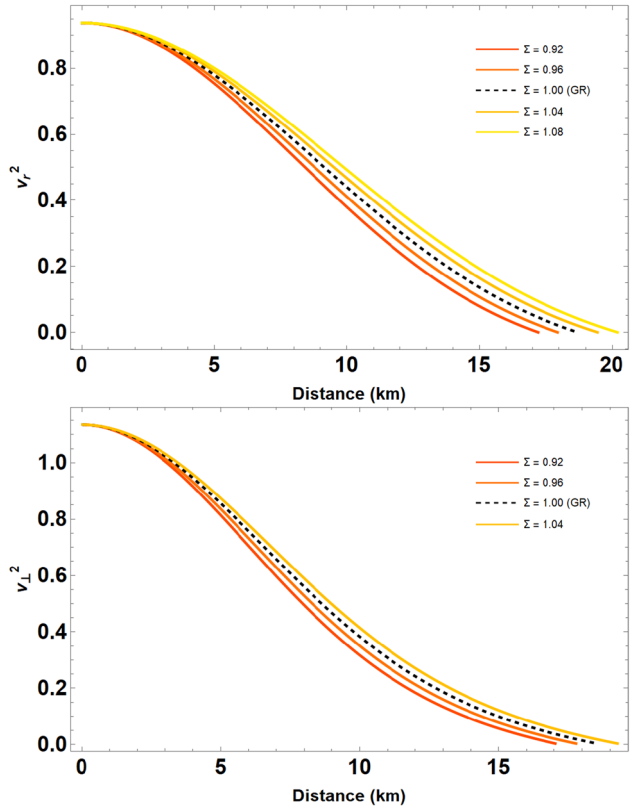

Fig. 7 The squared sound speed in the radial and tangential directions for anisotropic dark matter stars with variations in Σ

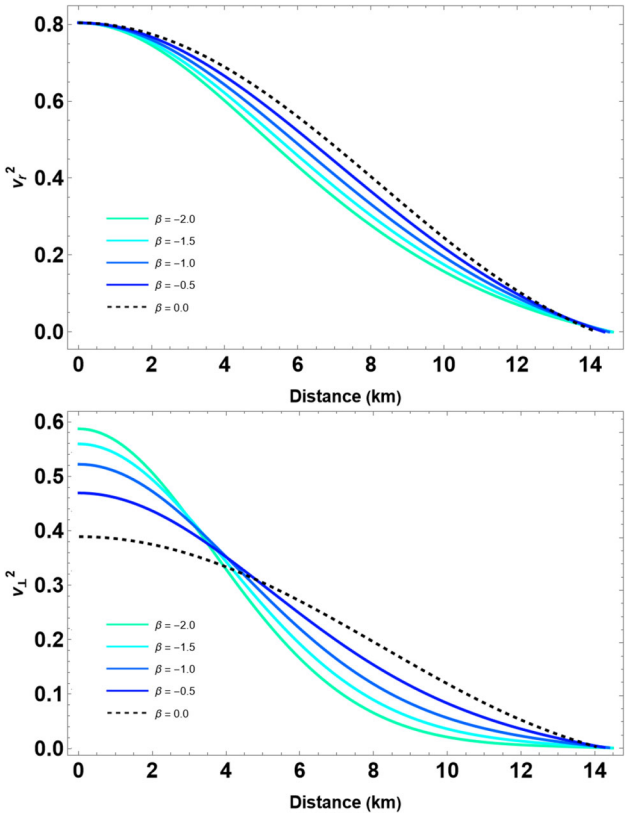

Fig. 8 The squared sound speed in the radial and tangential directions for anisotropic dark matter stars with variations in β

The findings confirm that the standard results regarding stellar stability remain valid within the framework of rainbow gravity. Specifically, all examined configurations adhere to the causality condition $v_{r,\perp}^2 < 1$, thereby confirming the physical viability and stability of the stellar models under consideration.

6 Concluding remarks

In this study, we investigated the structural and stability properties of anisotropic dark matter stars within the framework of gravity's rainbow. We began by formulating the field equations incorporating the energy-dependent rainbow functions $\Xi(x)$ and $\Sigma(x)$, which modify the spacetime geometry and dispersion relations at high energies. Using these modified equations, we derived the hydrostatic equilibrium conditions through a generalized TOV formalism. These equations, given in Eqs. (25)–(27), served as the foundation for exploring the properties of compact stars.

We analyzed the role of anisotropy, characterized by the difference between radial and tangential pressures, $\Delta = P_\perp - P_r$, in determining the equilibrium and stability of dark matter stars. Our results highlighted how the anisotropy parameter β and the rainbow parameter Σ influence key stellar properties such as mass, radius, and compactness. Figures 1 and 2 demonstrated the variations of energy density ρ, radial pressure P_r, and tangential pressure $P_\perp$ with respect to the radial coordinate r, under different parameter settings. We further examined the mass-radius and compactness relations, illustrated in Figs. 3 and 4, which showed that higher values of Σ and β led to more massive and compact stars. However, we are addressing a dark matter model; hence, the obtained isotropic solutions possess a greater mass than their anisotropic counterparts when $\beta < 0$ is considered (see Fig. 4).

To evaluate the stability of these stellar configurations, we applied the static stability criterion, adiabatic index analysis, and sound speed causality conditions. The $M - \rho_c$ curves in Fig. 4 confirmed that the stability regions are characterized by $dM/d\rho_c > 0$. Additionally, the adiabatic index γ satisfied the critical threshold $\gamma > 4/3$, as shown in Fig. 6, indicating dynamical stability. The sound speed analysis in Figs. 7 and 8 verified that the causality condition $v^2 < 1$ was upheld for all cases, further validating the physical feasibility of the solutions.

Despite the insights gained, our analysis is subject to certain limitations. The model assumes a static, spherically sym-

metric configuration, omitting effects such as rotation, magnetic fields, and dynamical evolution, which may influence compact star properties in realistic astrophysical settings. Additionally, while the adopted polytropic EoS serves as a reasonable approximation for dark-matter stars, alternative formulations, such as self-interacting bosonic condensates or non-minimally coupled dark-matter fields, could yield different equilibrium and stability characteristics [29,30]. Furthermore, the quantum gravitational corrections incorporated through the rainbow functions are phenomenological, rather than derived from a fundamental quantum gravity theory, limiting their predictive power beyond modified dispersion relations [11,13]. It is also insightful to compare rainbow gravity with alternative quantum gravity frameworks, such as asymptotic safety gravity, $f(R)$ gravity, and Horava-Lifshitz gravity. While asymptotic safety gravity introduces a running gravitational coupling that affects high-energy astrophysical environments [63], gravity's rainbow modifies the dispersion relation without requiring a running coupling constant. Similarly, $f(R)$ gravity modifies the Einstein–Hilbert action via higher-order curvature terms [9], leading to deviations from GR even in low-energy regimes. Horava–Lifshitz gravity, on the other hand, introduces anisotropic scaling between space and time, affecting field equations differently [64]. Unlike these approaches, rainbow gravity preserves compatibility with GR at low energies while incorporating quantum gravity-inspired deviations in the high-energy regime, making it particularly relevant for compact stars under extreme conditions. Addressing these aspects in future research will provide a more comprehensive understanding of the interplay between modified gravity, anisotropy, and dark matter in compact objects.

The increased maximum mass predicted by rainbow gravity provides a potential observational test of the modified TOV equations. Mass measurements of neutron stars, such as PSR J0740+6620 ($M \approx 2.08 M_{\odot}$) [65], serve as constraints on the model parameters. Additionally, deviations in the mass-radius relation can be probed through X-ray observations by NICER and future missions [66]. Moreover, gravitational wave signals from binary neutron star mergers, particularly post-merger oscillations, may exhibit modified frequencies due to quantum gravity effects [67], providing further avenues for testing rainbow gravity in astrophysical observation.

In future work, we aim to extend this study by exploring the role of different EoS and their impact on the interplay between anisotropy and quantum gravitational corrections. Additionally, incorporating rotational effects and magnetic fields in the framework of gravity's rainbow would provide deeper insights into the dynamics of compact stars. Observational constraints from gravitational wave data and high-precision pulsar timing will be integrated to refine the models and enhance their predictive capabilities.

Acknowledgements The authors express gratitude to the editor and anonymous referee for their insightful feedback, which greatly enhanced this manuscript. T. T. received support from Walailak University (Contract WU67268). İ.S. appreciates funding from TÜBİTAK, ANKOS, and SCOAP3. Both T. T. and İ.S. acknowledge networking support from COST Actions CA21106, CA22113, and CA23130. J.R. thanks Grant no. FA-F-2021-510 of the Uzbekistan Agency for Innovative Development.

Data Availability Statement This manuscript has no associated data. [Author's' comment: Data sharing is not applicable to this article, as no datasets were generated or analyzed during the current study.]

Code Availability Statement This manuscript has no associated code/software. [Author's comment: No software or code was generated or analyzed during the preparation of this manuscript.]

Funded by SCOAP[3].

References

1. S.K. Maurya, Y.K. Gupta, S. Ray, B. Dayanandan, Eur. Phys. J. C **75**, 225 (2015)
2. V. Cardoso, P. Pani, Living Rev. Relativ. **22**, 4 (2019)
3. C.G. Boehmer, T. Harko, Class. Quantum Gravity **23**, 6479 (2006)
4. Y. Feng, T. Naseer, G. Mustafa, S.K. Maurya, Eur. Phys. J. C **85**, 18 (2025)
5. E. Demir, T. Naseer, A. Ashraf, E. Güdekli, Chin. J. Phys. **91**, 299 (2024)
6. E. Berti, E. Barausse, V. Cardoso, L. Gualtieri, P. Pani, U. Sperhake, L.C. Stein, N. Wex, K. Yagi, T. Baker et al., Class. Quantum Gravity **32**, 243001 (2015)
7. T. Clifton, P.G. Ferreira, A. Padilla, C. Skordis, Phys. Rep. **513**, 1 (2012)
8. S. Nojiri, S.D. Odintsov, eConf C **0602061**, 06 (2006)
9. T.P. Sotiriou, V. Faraoni, Rev. Mod. Phys. **82**, 451 (2010)
10. G. Amelino-Camelia, Int. J. Mod. Phys. D **11**, 35 (2002)
11. J. Magueijo, L. Smolin, Class. Quantum Gravity **21**, 1725 (2004)
12. S.H. Hendi, G.H. Bordbar, B.E. Panah, S. Panahiyan, JCAP **09**, 013 (2016)
13. J. Kowalski-Glikman, arXiv:gr-qc/0603022
14. P.H.R.S. Moraes, G. Panotopoulos, I. Lopes, Phys. Rev. D **103**, 084023 (2021)
15. L. Herrera, W. Barreto, Phys. Rev. D **88**, 084022 (2013)
16. P. Jetzer, Phys. Rep. **220**, 163 (1992)
17. R. Brito, V. Cardoso, C.A.R. Herdeiro, E. Radu, Phys. Lett. B **752**, 291 (2016)
18. E. Sucu, İ Sakallı, Phys. Dark Univ. **47**, 101771 (2025)
19. T. Tangphati, İ. Sakallı, A. Banerjee, A. Pradhan, arXiv:2411.06170 [hep-th]

20. T. Tangphati, İ Sakallı, A. Banerjee, A. Pradhan, Phys. Dark Univ. **46**, 101610 (2024)
21. D.D. Doneva, S.S. Yazadjiev, Phys. Rev. D **85**, 124023 (2012)
22. H.O. Silva, C.F.B. Macedo, E. Berti, L.C.B. Crispino, Class. Quantum Gravity **32**, 145008 (2015)
23. D. Horvat, S. Ilijic, A. Marunovic, Class. Quantum Gravity **28**, 025009 (2011)
24. J.M.Z. Pretel, Eur. Phys. J. C **80**, 726 (2020)
25. A. Banerjee, İ Sakallı, B. Dayanandan, A. Pradhan, Chin. Phys. C **49**, 015102 (2025)
26. T. Tangphati, A. Banerjee, İ Sakallı, A. Pradhan, Chin. J. Phys. **90**, 422 (2024)
27. A. Banerjee, A. Pradhan, İ Sakallı, A. Dixit, Class. Quantum Gravity **42**, 025008 (2025)
28. A. Maselli, P. Pnigouras, N.G. Nielsen, C. Kouvaris, K.D. Kokkotas, Phys. Rev. D **96**, 023005 (2017)
29. M. Colpi, S.L. Shapiro, I. Wasserman, Phys. Rev. Lett. **57**, 2485 (1986)
30. P.H. Chavanis, T. Harko, Phys. Rev. D **86**, 064011 (2012)
31. A. Rahmansyah, A. Sulaksono, A.B. Wahidin, A.M. Setiawan, Eur. Phys. J. C **80**, 769 (2020)
32. A. Rahmansyah, A. Sulaksono, Phys. Rev. C **104**, 065805 (2021)
33. P.H.R.S. Moraes, G. Panotopoulos, Phys. Rev. D **103**, 084023 (2021)
34. E.W. Mielke, F.E. Schunck, Nucl. Phys. B **564**, 185 (2000)
35. C.A.R. Herdeiro, E. Radu, H. Runarsson, T. Terni, Phys. Rev. D **105**, 044058 (2022)
36. C.A.R. Herdeiro, G. Panotopoulos, E. Radu, JCAP **08**, 029 (2020)
37. R. Ruffini, S. Bonazzola, Phys. Rev. **187**, 1767 (1969)
38. F.E. Schunck, E.W. Mielke, Class. Quantum Gravity **20**, R301 (2003)
39. E. Seidel, W.M. Suen, Phys. Rev. Lett. **66**, 1659 (1991)
40. D.J. Kaup, Phys. Rev. **172**, 1331 (1968)
41. F.V. Kusmartsev, E.W. Mielke, F.E. Schunck, Phys. Rev. D **43**, 3895 (1991)
42. S.L. Liebling, C. Palenzuela, Living Rev. Relativ. **15**, 6 (2012)
43. C.F.B. Macedo, P. Pani, V. Cardoso, L.C.B. Crispino, Phys. Rev. D **88**, 064046 (2013)
44. V. Cardoso, E. Franzin, A. Maselli, P. Pani, G. Raposo, Phys. Rev. D **95**, 084014 (2017)
45. T. Rindler-Daller, P.R. Shapiro, Mod. Phys. Lett. A **29**, 1430002 (2014)
46. L. Hui, J.P. Ostriker, S. Tremaine, E. Witten, Phys. Rev. D **95**, 043541 (2017)
47. L.Q. Su, C. Shi, Y.F. Huang, Y. Yan, C.M. Li, W.L. Yuan, H.S. Zong, Astrophys. Space Sci. **369**, 29 (2024)
48. Y. Bai, A.J. Long, JHEP **06**, 072 (2018)
49. C. Cattoen, T. Faber, M. Visser, Class. Quantum Gravity **22**, 4189 (2005)
50. V. Folomeev, Phys. Rev. D **97**, 124009 (2018)
51. K. Yagi, N. Yunes, Phys. Rev. D **91**, 123008 (2015)
52. P. Mazur, E. Mottola, Proc. Natl. Acad. Sci. **101**, 9545 (2004)
53. R.A. Konoplya, A. Zhidenko, Rev. Mod. Phys. **83**, 793 (2011)
54. B.K. Harrison, *Gravitational Theory and Gravitational Collapse* (University of Chicago Press, Chicago, 1965)
55. Y.B. Zeldovich, I.D. Novikov, Relativistic astrophysics. Vol.1: Stars and relativity (University of Chicago Press, Chicago, 1971)
56. T. Tangphati, A. Pradhan, A. Errehymy, A. Banerjee, Ann. Phys. **430**, 168498 (2021)
57. H. Maulana, A. Sulaksono, Phys. Rev. D **100**, 124014 (2019)
58. Y.H. Sham, L.M. Lin, P.T. Leung, Phys. Rev. D **86**, 064015 (2012)
59. J.M.Z. Pretel, A. Banerjee, A. Pradhan, Eur. Phys. J. C **82**, 180 (2022)
60. S. Chandrasekhar, Astrophys. J. **140**, 417 (1964)
61. A. Banerjee, A. Pradhan, B. Dayanandan, A. Ali, Eur. Phys. J. C **84**, 730 (2024)
62. E.N. Glass, A. Harpaz, Mon. Not. R. Astron. Soc. **202**, 1 (1983)
63. R. Percacci, *An Introduction to Covariant Quantum Gravity and Asymptotic Safety* (World Scientific, Singapore, 2017)
64. P. Hořava, Phys. Rev. D **79**, 084008 (2009)
65. H.T. Cromartie et al., Nat. Astron. **4**, 72 (2020)
66. M.C. Miller et al., Astrophys. J. Lett. **887**, L24 (2019)
67. B.P. Abbott et al. [LIGO Scientific and Virgo Collaborations], Phys. Rev. Lett. **119**, 161101 (2017)